Characterization of Dynamics of Gas–Liquid Flows in Rectangular Bubble Columns

Vivek V. Buwa and Vivek V. Ranade
Industrial Flow Modeling Group, National Chemical Laboratory, Pune 411 008, India

Gas–liquid flow in bubble columns is inherently unsteady. The unsteady fluid dynamics influences mixing and other transport processes occurring in bubble column reactors. In this work, we have characterized dynamics of gas–liquid flows in rectangular bubble columns using wall pressure and voidage fluctuations. The low-frequency oscillations caused by meandering bubble plume were characterized using the plume oscillation period. Experiments were carried out to study the influence of superficial gas velocity, sparger configuration, and liquid height-to-width (H/W) ratio on the low-frequency oscillations. The dimensional analysis based on analogy between buoyancy-driven thermal and bubbly flows was carried out to relate low-frequency oscillations to various design and operating parameters. This analysis was able to correlate present as well as previously published experimental data. We have further demonstrated the importance of establishing such a quantitative relationship for validation of computational fluid dynamics (CFD)–based models by carrying out CFD simulations of gas–liquid flow in rectangular bubble columns. The importance of bubble-scale information obtained using conductivity probes in validating Eulerian–Lagrangian models is also demonstrated. © 2004 American Institute of Chemical Engineers AIChE J, 50: 2394–2407, 2004
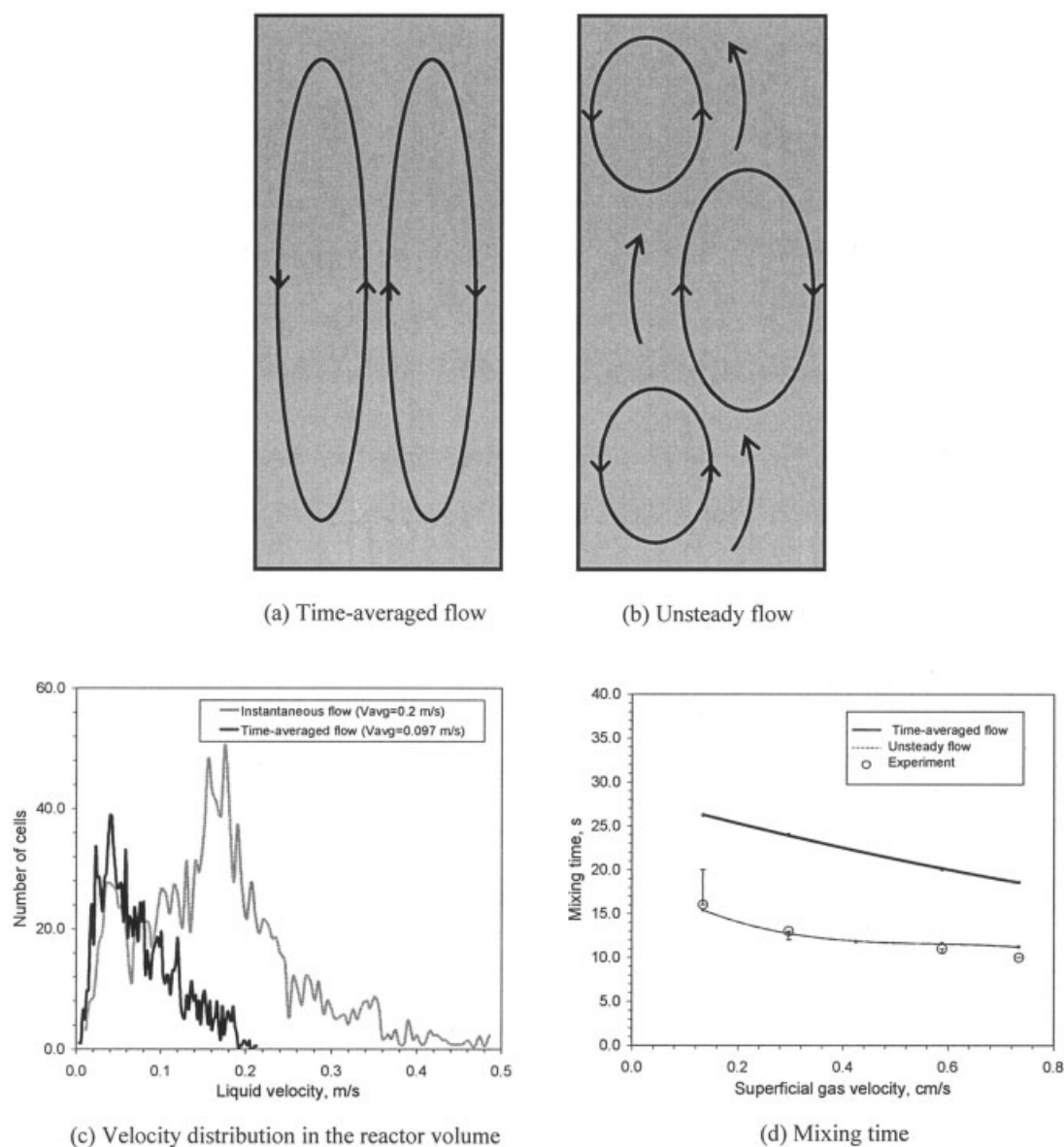*Keywords: bubble column, gas–liquid flows, dynamics, CFD*

Introduction

Bubble columns are widely used in chemical and allied industries. The gas–liquid flow in a bubble column is inherently unsteady and consists of a variety of flow processes occurring with different length and time scales. On one hand, the meandering bubble plume causes macroscopic recirculatory flow, consisting of several ascending and descending vortical structures with dimensions of the order of the column width and frequencies of the order of 10^{-1}–10^{0} Hz. On the other hand, bubble-scale flow (vortices shed by bubbles, flow around individual bubble, bubble–bubble interaction) has very different characteristic length and time scales (length scale of the order of bubble diameter and frequencies of the order of 10^{0}–10^{1} Hz). The overall dynamics is the result of interactions of these flow processes. The unsteady fluid dynamics, which influences mixing and transport processes occurring in bubble column reactors, is a complex function of design and operating parameters such as reactor configuration, sparger, and gas flow rate. Several attempts have been made to understand and to characterize the complex fluid dynamics of bubble columns.

Most of the earlier work was focused on characterization of time-averaged flow behavior (up-flow in the center of column and down-flow near the column walls, as shown schematically in Figure 1a) by measurement of time-averaged gas holdup and liquid velocity profiles (for example, Kumar et al., 1997; Yao et al., 1991, and references cited therein). Although these experimental and computational efforts were useful in providing overall guidelines for reactor design, they failed to capture unsteady recirculatory flow structures in bubble columns. Chen et al. (1994) observed that the transient recirculatory flow structures in bubble columns are significantly different from the gross recirculation observed in time-averaged flow measurements (see Figure 1b). Recently, Buwa and Ranade (2003)

Correspondence concerning this article should be addressed to V. V. Ranade at vvranade@ifmg.ncl.res.in.

(a) Time-averaged flow   (b) Unsteady flow

(c) Velocity distribution in the reactor volume   (d) Mixing time

Figure 1. Role of unsteady fluid dynamics in mixing in bubble columns.

showed computationally that the liquid velocity distribution in the reactor volume for time-averaged flow and instantaneous transient flow is significantly different (shown in Figure 1c). It can be seen that for any instantaneous flow field, a significant portion of the bubble column has much larger velocities than those observed for the time-averaged flow field. Buwa and Ranade (2003) observed that the mixing time values predicted using time-averaged flow field are much larger than the experimentally observed values. Predictions based on unsteady flow agree very well with the experimental data (see Figure 1d). It is thus essential to understand unsteady flow characteristics of gas–liquid flows in bubble columns.

Several attempts were previously made to characterize unsteady flows in bubble columns experimentally (see, for example, Becker et al., 1999; Chen et al., 1994; Pfleger and Becker, 2001). Although these studies were useful in developing qualitative understanding of dynamic characteristics, adequate

quantitative information on how these unsteady characteristics relate to design and operating parameters is not available. The main difficulty in characterizing gas–liquid flow in bubble columns is that the flow becomes opaque at a higher gas volume fraction and renders the photographic or optical techniques such as laser Doppler anemometry (LDA) and particle image velocimetry (PIV) unusable. Under such circumstances, pressure sensors and conductivity probes offer simple, cost-effective, and robust measurement techniques. In the present work, we have therefore used wall pressure fluctuations and voidage fluctuations to characterize the dynamics of various flow processes.

Several attempts have also been made recently to computationally investigate unsteady dynamics of gas–liquid flows in bubble columns (see, for example, Buwa and Ranade, 2002 and references cited therein). Most of the computational studies modeled flow in a rectangular bubble column. The interest in

Table 1. Review of Previous Work on Experimental Characterization of Dynamics of Gas–Liquid Flows in Bubble Columns

Authors	Column Geometry $(W \times D \times H)$ (cm)	Superficial Gas Velocity (cm/s)	Parameters Studied	Measured Parameters
	Visual observations			
Chen et al. (1989)	$76 \times 5 \times 120$* $17.5 \times 1.5 \times 180$*	3.5	U_G, H/W ratio	Visualization of unsteady flow structures
Tzeng et al. (1993)	$48.3 \times 1.27 \times 160$*	0.5–6.4	U_G, Gas injectors	Visualization of unsteady flow structures
Delnoij et al. (1997)	$25 \times 2 \times 200$*	0.2–0.6	U_G, H/W ratio	Plume oscillation frequency
	Particle image velocimetry			
Chen et al. (1994)	$10.2D$, $120H$**	0.1–5.5	Flow regimes	—
Lin et al. (1996)	10.16, 15.24, 20.32, 30.48, $48.26 \times 1.27 \times 160$* $60.96 \times 0.64 \times 229$*	0.1–6.0	U_G, Column width	Flow structures, vortex size, wavelength, and frequency of vortical structures
	Laser Dopler anemometry			
Becker et al. (1994)	$50 \times 8 \times 200$*	0.0666	—	Plume oscillation frequency
Becker et al. (1999), Pfleger (2000)	$20 \times 5 \times 45$* $29.5D \times 250H$**	0.0695–0.60 0.15–2.0	U_G	Plume oscillation frequency
Pfleger and Becker (2001)	$29.5D \times 250H$**	2.0	U_G	Plume oscillation frequency
	Pressure fluctuations			
Drahos et al. (1991)	$29.2D \times 120H$**	2.5–16.6	U_G	Flow regime identification
Letzel et al. (1997)	10, $19D \times 200H$**	0.0–30.0	U_G, H/D ratio	Flow regime identification
Vial et al. (2000)	$10D \times 200H$**	0.6–15	U_G, Sparger	Flow regime identification
Buwa and Ranade (2002)	$20 \times 5 \times 90$*	0.16–0.83	U_G, sparger, bubble size	Plume oscillation frequency
Rampure et al. (2003)	$20D \times 200H$**	1–30	U_G	Characteristic timescale of low-frequency oscillations
	Optic probes			
Rensen and Voig (2001)	$15 \times 15 \times 67$*	0.095–0.64	U_G	Plume oscillation frequency, plume width
	Wall pressure and voidage fluctuations			
Present study	$20 \times 5 \times 120$*	0.16–14.0	U_G, Sparger configuration, H/W ratio	Plume oscillation frequency, bubble passage frequencies, dimensional analysis

All experiments were carried out for air–water system.
 *Rectangular column.
**Cylindrical column.

rectangular bubble columns, however, is not just for academic reasons. Rectangular bubble column retains all the key characterisics of cylindrical bubble columns and allows systematic and quick computational fluid dynamics (CFD) simulations resulting from lower demands on computational resources. CFD models, validated using the data on rectangular bubble columns, would be applicable to simulate flow in cylindrical bubble columns as well and would therefore be useful for practical applications. Unfortunately, adequate data on unsteady flow characteristics are not available even for rectangular bubble columns. No clear understanding of the influence of parameters, such as sparger, bubble size, and height-to-width ratio on dynamics of gas–liquid flows, is available. Under such circumstances, the computational models are validated by using data collected on just one set of key design parameters.

The present work was undertaken with an objective to understand the dynamics of various flow processes (low-frequency oscillations and bubble-scale processes) and to develop a quantitative relationship between the characteristics of low-frequency oscillations and various design and operating parameters. A brief review of previous work on experimental characterization of dynamics of gas–liquid flows in bubble columns is presented in the following subsection. In light of this review,

the specific contributions of the present work and the organization of this article are discussed.

Previous work

Most of the published work on dynamics of gas–liquid flows was focused on stability and on identifying regime transitions of buoyancy-driven flows (see, for example, Ruzicka and Thomas, 2003 and references cited therein). Because the key objective of the present work is to characterize low-frequency oscillations of gas–liquid flows, the vast literature on stability and regime transition is not reviewed here. The previous work, relevant to the present study, is summarized in Table 1. Low-frequency oscillations were observed for cylindrical bubble columns (see, for example, Chen et al., 1994; Drahos et al., 1991; Letzel et al., 1997; Pfleger and Becker, 2001, Rampure et al., 2003; Ranade and Utikar, 1999; Ruzicka et al., 2000; Vial et al., 2000). In most of these studies, pressure fluctuations were used to characterize flow regimes in bubble columns. These experimental studies indicate that the low-frequency oscillations corresponding to local recirculatory flow occur with frequencies less than 1.0 Hz. However, no systematic information is available on the characteristics of these low-

frequency oscillations and how these change with key design and operating parameters. Compared to the cylindrical bubble columns, the dynamics of rectangular columns was studied more extensively, which is reviewed below.

Chen et al. (1989) and Tzeng et al. (1993) visually studied the local recirculatory flow structures in rectangular bubble columns. Chen et al. (1994) used particle image velocimetry to study various flow regimes. Lin et al. (1996) studied the effect of superficial gas velocity and column width on vortex size, wavelength, and oscillation frequency of vortical flow structures. Their results indicate that the wavelength of vortices decreases with increase in superficial gas velocity and becomes independent of gas velocity for the coalesced bubble (or churn-turbulent) regime. The bubble plume oscillation frequency was found to depend on column diameter and superficial gas velocity. Delnoij et al. (1997) measured the plume oscillation frequency at very small gas flow rates using video recording. They found that the plume oscillation frequency was independent of height-to-width (or diameter), H/W, ratio. Recently, laser Doppler anemometry (Becker et al., 1994, 1999; Pfleger, 2000) was used to measure the local liquid velocity time series, which was further used to measure plume oscillation frequency. However, most of these studies were limited to just one particular column and sparger configuration. Buwa and Ranade (2002) studied the effect of superficial gas velocity, sparger configuration, and bubble size on low-frequency oscillations using wall pressure fluctuation measurements for low superficial gas velocities (in the range of 0.16 to 0.83 cm/s).

Rensen and Voig (2001) analyzed the motion of a confined bubble plume in a rectangular bubble column using optic probes and presented dimensionless frequencies [defined by Strouhal number (f^*)] as a function of Rayleigh number (Ra) based on the analysis of Kimura and Iga (1995), defined as

$$f^* = \frac{fL_i}{U_G} \qquad \text{and} \qquad \text{Ra} = \frac{\rho g L_i^2 U_G}{\mu U_B^2} \qquad (1)$$

where f is the measured plume oscillation frequency, U_G is the superficial gas velocity, U_B is the bubble rise velocity, and L_i is the initial plume width (which was equal to the width of sparger area).

We have analyzed the data available in the literature using these dimensionless numbers. Because Lin et al. (1996) used multiple tube injectors, placed equidistant over the entire column width, L_i was set equal to the width of the column (W). Superficial gas velocity calculated based on the entire cross-sectional area of column was used. Following Rensen and Voig (2001), a constant bubble rise velocity of 30 cm/s was used. It was observed that the dimensional analysis carried out by Rensen and Voig (2001) could not unify the effect of column width on the plume oscillation frequency as observed by Lin et al. (1996). Even though Rensen and Voig (2001) argued that the oscillation frequency depends on sparger width and bubble size, neither qualitative nor quantitative data are available. Therefore, further experiments are clearly needed to establish the quantitative relationship between plume oscillation frequency and key design and operating parameters.

Present contribution

In the present work, we have used wall pressure and voidage fluctuations to study the influence of superficial gas velocity, sparger configuration, and liquid height-to-width ratio on low-frequency oscillations. The superficial gas velocities were varied from 0.16 to 14.0 cm/s. The low-frequency oscillations caused by a meandering bubble plume were characterized using the measured plume oscillation period. Voidage fluctuations were used to characterize the low-frequency oscillations and bubble-scale processes. The dimensional analysis based on analogy between buoyancy-driven thermal and bubbly flows was carried out to relate low-frequency oscillations to various design and operating parameters. The analysis was used to unify the present as well as previously published experimental data. The experimental setup, wall pressure, and voidage fluctuation measurements are presented in the following section. The results from wall pressure and voidage fluctuation measurements are discussed thereafter.

Experimental
Setup

A rectangular bubble column of 0.2 m width, 1.2 m height, and 0.05 m depth was set up (see Figure 2a). This geometry is the same as that used by Pfleger et al. (1999). All experiments were carried out using air as a sparged gas. The superficial gas velocity was varied from 0.16 to 14.0 cm/s. Tap water was used as a liquid phase unless mentioned otherwise. Buwa and Ranade (2002) carried out initial experiments using a standard sparger (sparger 1 in Table 2) at superficial velocities in the range of 0.16 to 0.83 cm/s and at H/W ratio of 2.25 to benchmark the experimental technique and procedure against LDA measurements of Pfleger et al. (1999). They also studied the effect of sparger configuration on dynamic characteristics, using spargers of different hole diameters and pitches (spargers 1–6 in Table 2) for superficial gas velocity in the range of 0.16 to 0.83 cm/s. In the present work, we have further studied the effect of partly and fully aerated spargers (spargers 7 and 8) on the dynamic characteristics for superficial gas velocities in the range of 0.16 to 14.0 cm/s. The effect of liquid height (H) to column width (W) ratio was also studied by carrying out experiments at H/W ratio of 1.125, 3.375, 4.5, and 5.5. Voidage fluctuation measurements were carried out using a standard sparger (sparger 1 of Table 2). The experiments were carried out using the standard sparger at H/W ratio of 2.25, unless specified otherwise.

The average bubble size produced by different spargers was measured using a high-speed digital imaging system (Red Lake Imaging, San Diego, CA), which can acquire images at a rate as high as 500 frames/s. The digitized images were analyzed using the commercial software Image Pro Plus (Media Cybernetics, Silver Spring, MD) to calculate the bubble size distribution (Buwa and Ranade, 2002).

Wall pressure fluctuation measurements

Two pressure transducers (with range of ± 34.46 kPa, resolution of 0.000482 kPa, and sensitivity of 72.54 mV/kPa) were used (Model 106B50; PCB Piezotronics, Depew, NY) to measure wall pressure fluctuations. The pressure sensors were mounted flush on the sidewall of the column at
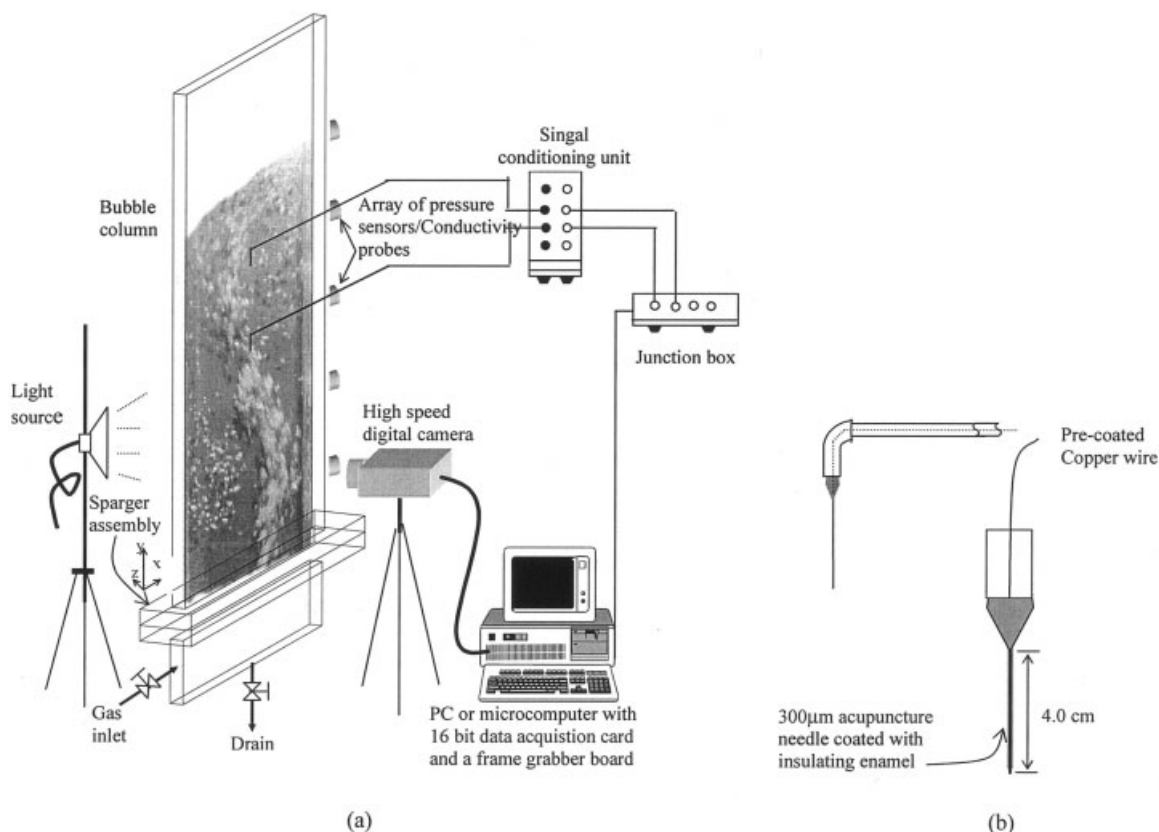
Figure 2. (a) Experimental setup for characterization of gas–liquid flows in a rectangular bubble column; (b) probe design.

various positions along the height of the column. The transducers were powered by ICP battery units (Model 480E06; PCB Piezotronics), which also act as amplifiers. The amplified signal was acquired using a microcomputer with a 16-bit A/D PCMCIA converter card and the data-acquisition software dAtagate (of nCode International, Sheffield, U.K.). In experiments carried out to measure the plume oscillation period, the pressure fluctuation signal was acquired with a sampling frequency of 15.0 Hz for 1200 s and filtered with a low-pass frequency of 1.0 Hz. Buwa and Ranade (2002) showed the typical raw and filtered signal together with corresponding power spectrum and discussed data processing in detail. Acquired time series of pressure fluctuations were analyzed using the AnTS (Analysis of Time Series) software (Sunthankar and Ranade, 1997).
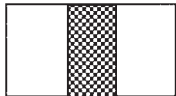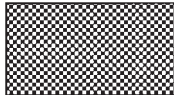
The plume oscillation period was calculated as the reciprocal of the characteristic frequency corresponding to motion of the meandering plume. Even though the accuracy of characteristic frequency depends on the number of bins used for calculation of power spectral frequency, the maximum error in plume oscillation period obtained by using 512 bins is less than 4% (compared to the value obtained with 8192 bins). At low superficial gas velocities, motion of the bubble plume was found to be quasi-periodic and a single value of characteristic low frequency was observed. However, at higher gas velocities, the flow behavior becomes increasingly chaotic. Under such circumstances, although dominant low-frequency peaks are observed, it is difficult to charac-

terize the motion of bubble plume with a single value of characteristic frequency attributed to scattered peaks. Other methods such as rescale range analysis (R/S) or their modified variants like V-statistic or P-statistic (Briens and Briens, 2002), which give a single value of characteristic timescale, were not found to be useful in characterizing low-frequency oscillations. In the present work, therefore, mean cycle time (reciprocal of mean oscillation frequency) was used to characterize low-frequency oscillations at higher gas velocities ($>$1.67 cm/s). The mean oscillation frequency was calculated as the ratio of first- and zero-order moment of power spectral density function integrated from zero to characteristic low frequency (peaks with frequency $<$ 1.0 Hz in the present work) as

$$\bar{f}_{\text{low freq}} = \frac{\int_0^{f_{\text{low freq}}} fP(f)df}{\int_0^{f_{\text{low, freq}}} P(f)df} \tag{2}$$

where $P(f)$ is the power contained in the frequency range of f and $f + df$.

Table 2. Details of the Spargers Used in the Present Work

Sparger		Configuration				
		Code	Location	No. of Orifice N_h	Diameter d_h (mm)	Pitch, P (mm)
Locally aerated	Spargers 1 to 5					
		1 Standard	Center	8	0.8	6
		2 Large pitch	Center	8	0.8	12
		3 Large hole	Center	8	1.2	6
		4 Large hole/ Large pitch	Center	8	1.2	12
	Sparger 6	5 Coalescing	Center	8	2.0	3
		6 Sintered disc	Center	Sintered disc, 18×6 mm^2 area		
Partly aerated	Sparger 7	7 Partly aerated	8×5 cm at center (% free area: 0.32)	64	0.8	6
Fully aerated	Sparger 8	8 Fully aerated	Entire cross section (% free area: 1.28)	256	0.8	6

Voidage fluctuation measurements

Conductivity probes were developed using silver-coated acupuncture needles having a diameter of 300 μm. The tapered end of the needle makes it ideal for bubble piercing. The other end of the needle was connected to insulated copper wire and was carried through a rigid tube (diameter 3.0 mm, length 30 cm), which acts as a support to the copper wire (see Figure 2b). A thin coat of insulating enamel ($\sim$ 25 μm) was applied to the needle surface and other joints, which makes it electrically insulating. The enamel from the tip of the insulated needle, which acts as the sensing point, was removed by scratching. The measurements were carried out at different locations along the height of the column using ports provided on the sidewall of the column (in the Y-direction). Probe position in the transverse direction (X-direction) was adjusted by moving the copper tube through these ports, positioned with ± 1 mm accuracy. Appropriate signal conditioning electronics was developed to ensure adequate response and resolution without obtaining wiggles or baseline drift (Buwa et al., 2001). The amplified signal was acquired using a microcomputer with a 16-bit A/D PCMCIA converter card and data-acquisition software dAtagate (both from nCode International).

The voidage signal was acquired through a conductivity probe with a sampling frequency of 5 kHz and is shown elsewhere (see Buwa, 2004). Such high data-acquisition rates were necessary to ensure that measured gas holdup values were independent of the sampling frequency. The acquired time series of voidage fluctuations was processed and analyzed using an in-house code vFAT (voidage fluctuation analysis tool). The signal baseline was first corrected to zero and then the signal was normalized on a 0 to 1 scale by using global maximum voltage attained by any peak during the entire time series (see Buwa, 2004). The raw signal contains spurious high-frequency noise and needs to be selectively removed using appropriate noise threshold (NT). After removing the high-frequency noise, the raw signal peaks need to be converted into square peaks using an appropriate phase discrimination threshold (PDT). A typical phase-discriminated signal using a PDT of 5% of local peak height is shown in Figure 3. The phase marker function $M(x, t)$ is defined as

$$M(x, t) = 1 \quad \text{if gas at position } x \text{ at time } t$$
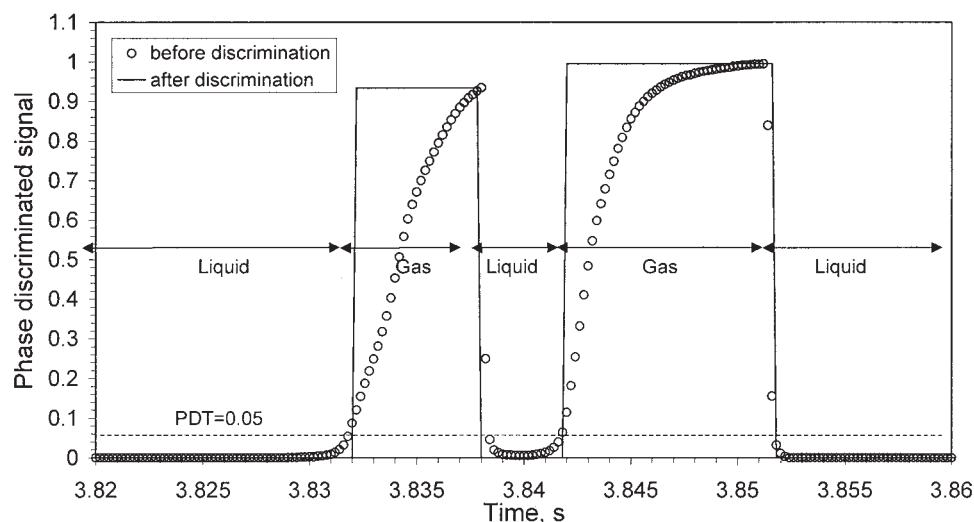$$= 0 \quad \text{if liquid at position } x \text{ at time } t \quad (3)$$

Figure 3. Typical signal before and after phase discrimination.

Thus, gas holdup averaged over a period T at any point x can be calculated as

$$\bar{\varepsilon}_G = \frac{1}{T} \int_0^T M(x,\,t)dt \qquad (4)$$

The time-averaged gas holdup was calculated using different values of NT, varying from 0 to 100% for different gas flow rates. It was observed that because of the presence of high-frequency noise with normalized amplitude less than 1% (of maximum amplitude observed in the entire time series), the calculated values of time-averaged gas holdup decrease sharply with NT up to 1%. With further increases in NT, the gas holdup becomes a slow varying function of NT. Thus, the value of NT was set to 1% in the present work. Separate calibration experiments were carried out using a small rectangular column [5 × 50 × 2 cm (width × height × width)]. The time-averaged gas holdup, measured using high-speed imaging, was compared with that obtained using probes with different values of PDT. It was observed that a PDT of 10% could predict the gas holdup measured by photography within ±13% for superficial gas velocity up to 0.63 cm/s. Thus, a PDT of 10% was used in further calculations of gas holdup. Details of probe calibration experiments are not included for the sake of brevity. Number of bubbles, average number of data points per bubble peak, time-averaged gas holdup, local voidage fluctuations, and distribution bubble passage frequency were computed using vFAT.

Results and Discussion

When gas is introduced into the column filled with liquid, bubbles formed at sparger holes rise upward through the pool of liquid. At small gas throughputs, a meandering chain of bubbles was observed. With further increase in gas through-puts, the local unsteady flow around individual bubbles and their interaction with other bubbles manifests into low-frequency oscillations superimposed with oscillations generated by bubble-scale processes. The overall dynamics is the result of interactions of these flow processes. The dynamics of these flow processes can be characterized by analyzing temporal behavior of key variables such as wall pressure or local gas holdup. In the following, we first discuss wall pressure fluctuation measurements and dimensional analysis. Later, we discuss results of voidage fluctuation measurements.

Wall pressure fluctuations measurements

In our earlier work (Buwa and Ranade, 2002), we compared the plume oscillation period measured by wall pressure fluctuation measurements with the LDA measurements of Pfleger (2000), to benchmark our measurement technique and experimental procedure. Buwa and Ranade (2002) carried out wall pressure fluctuation measurements in a rectangular bubble column with H/W ratio of 2.25 using different locally aerated spargers for superficial gas velocities in the range of 0.16 to 0.83 cm/s. The effect of sparger configuration on the plume oscillation period was studied for spargers 1 to 6 (listed in Table 2). It was observed that the measured plume oscillation period was not sensitive to the pitch and hole diameter (for pitch > 3 mm and hole diameter ≤ 1.2 mm, spargers 2–4 in Table 2). However, they found that the plume oscillation period was not influenced directly by the sparger configuration, but affected the plume oscillation period through the bubble size distribution produced by individual spargers. They further verified the role of bubble size in dynamic characteristics by conducting experiments in the presence of alcohol (which reduces surface tension and suppresses coalescence and thus reduces average bubble size).

In this work, we have carried out wall pressure measurements to study the effect of superficial gas velocity using partly and fully aerated sparger (spargers 7 and 8 in Table 2) with 0.32 and 1.28% free area for superficial gas velocities in the range of 0.16 to 14.0 cm/s and results are shown in Figure 4a. Because the bubble size distribution observed for a partly aerated sparger was similar to that for a standard sparger (because both had the same hole diameter and pitch), the plume oscillation periods were the same as those observed for the standard sparger. It was observed that the plume oscillation period decreases sharply up to superficial gas velocity of 0.83 cm/s. It should be noted that the slopes for these two parts are
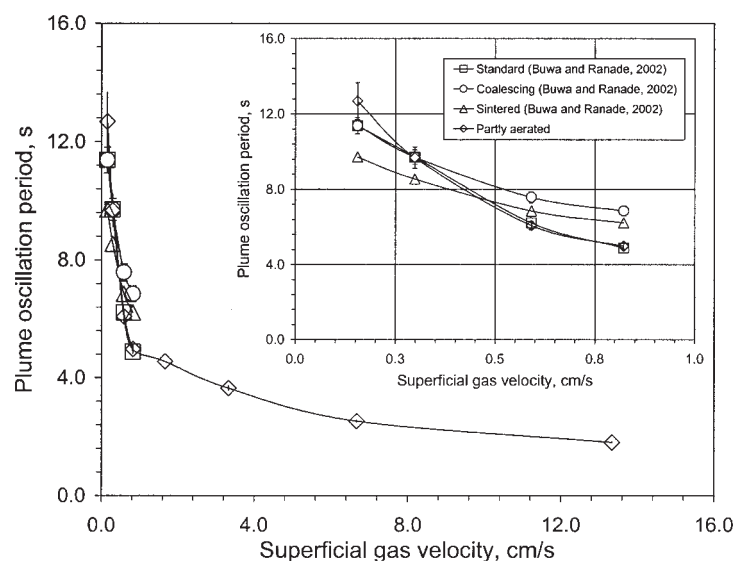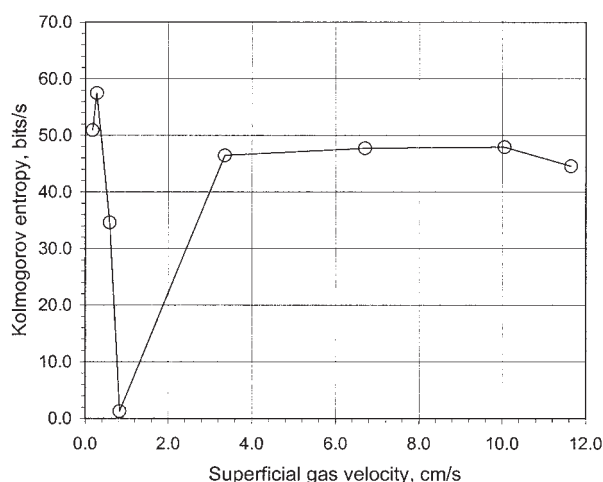
Figure 4. (a) Effect of sparger configuration on plume oscillation; (b) Kolmogorov entropy for partly aerated sparger (*H/W* = 2.25).

almost the same (on a log–log scale) and the plume oscillation time is proportional to the reciprocal of square root of superficial gas velocity (see following section on dimensional analysis for detailed discussion). This variation in slopes appears to be attributed to the flow regime transition from homogeneous bubbly flow to coalesced bubble (churn-turbulent) flow for superficial gas velocity in the range of 0.83 to 1.16 cm/s. To verify this further, following Utikar et al. (2001), we have calculated Kolmogorov entropy of the wall pressure fluctuation time series acquired for superficial gas velocities in the range of 0.16 to 11.67 cm/s, as shown in Figure 4b. The flow regime transition is indicated by a sharp decrease in the Kolmogorov entropy values.

For the fully aerated sparger (sparger 8), no oscillatory plume behavior was observed. The gas bubbles rise from one of the column sidewalls, generating a large circulation cell, which covers almost the entire column cross-sectional area. The wall pressure fluctuation time series was acquired at two different ports along the column height with constant liquid height. The measured plume oscillation period was found to be independent of the location of pressure sensor. The effect of *H/W* ratio on plume oscillation period is shown in Figure 5 for a sintered disc sparger (sparger 6). It can be seen that there is no significant difference in the plume oscillation period with increase in the *H/W* ratio except at low gas velocity. Similar results were observed for a standard sparger.

Dimensional analysis

We have extended the analogy between the buoyancy-driven thermal and bubbly layers presented by Ruzicka and Thomas (2003) using suitably modified definitions of Strouhal and Rayleigh numbers. The dimensionless frequency is defined using Strouhal number as (Rensen and Voig, 2001)
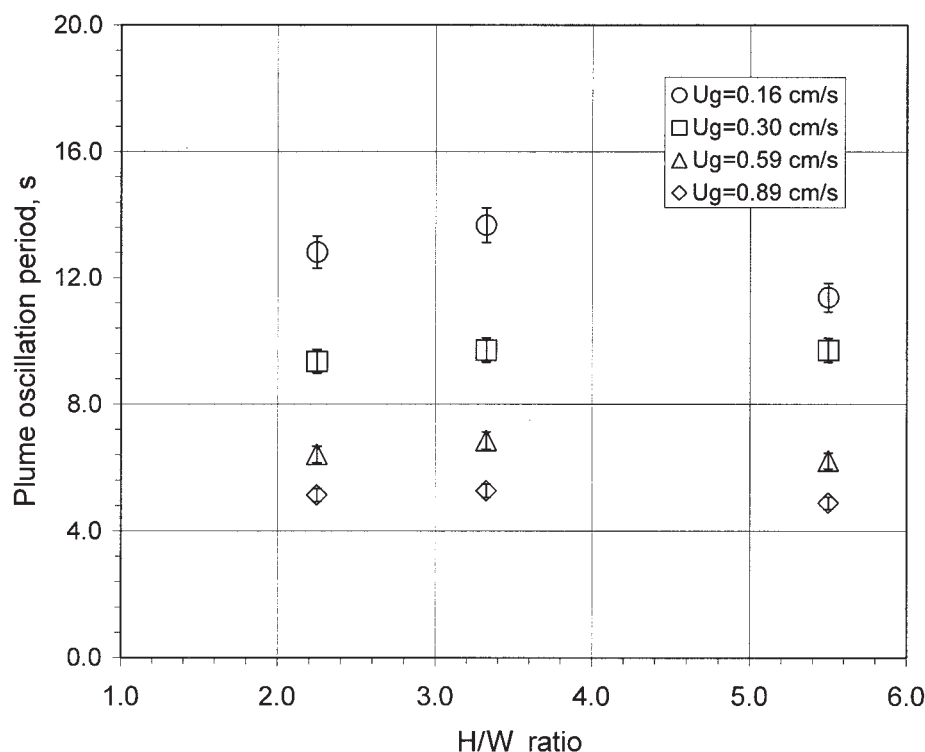
Figure 5. Effect of *H/W* ratio on plume oscillation period for sintered disc sparger.

$$f^* = \frac{fW}{U_G} \qquad (5)$$

where f is the characteristic frequency corresponding to the oscillatory motion of a meandering bubble plume, W is the width of the column, and U_G is the superficial gas velocity. The Rayleigh number is defined as the ratio of the buoyancy force $[F_b = g\rho_L\varepsilon_G(\tau_H/\tau_v)]$ and viscous force $[F_v = \mu(U_B/d_B^2)]$. The term τ_H/τ_v in the buoyancy force is the efficiency factor (see Ruzicka and Thomas, 2003). In the present work, we have defined τ_H as the characteristic time scale corresponding to the lateral dispersion of bubbles, which was estimated as $\tau_H = l^2/\Gamma$, where l is the characteristic length relevant to dispersion of a bubble, which was taken as the diameter of a bubble (d_B). Following Sato et al. (1975), the dispersion coefficient (Γ) was defined as the product of characteristic velocity (U_B) and characteristic length scale (d_B). With these substitutions, τ_H becomes $\tau_H = d_B/U_B$. τ_v was defined as the characteristic time scale corresponding to the recirculatory motion of a typical circulation cell (that is, the time required for the bubble to travel one circulation scale with characteristic length of column width), $\tau_v = W/U_B$. Here, d_B, W, and U_B are bubble diameter, column width, and bubble rise velocity, respectively. The gas volume fraction (ε_G) may be approximated as U_G/U_B. Using these definitions, the Rayleigh number thus becomes

$$Ra = \frac{g\rho_L U_G d_B^3}{\mu W U_B^2} \qquad (6)$$

The Strouhal and Rayleigh numbers defined by Eqs. 5 and 6 are plotted for experimental data reported above and for data in

the literature, as shown in Figure 6. In the above analysis, the Strouhal and Rayleigh numbers were calculated using measured average bubble sizes of 5 mm for tap water and 2.5 mm in the presence of butanol. In the absence of reliable data on bubble size at different superficial gas velocities, the variation of bubble size with superficial gas velocity could not be confirmed. The corresponding bubble rise velocities of 0.2 and 0.12 m/s, respectively, were used in the above analysis. This may be one of the possible sources of scatter of points around the trend line. From the data presented in Figure 6, f^* was found to vary with Ra as

$$f^* = \frac{5.0}{\sqrt{Ra}} \qquad (7)$$

From the results presented above and reported in the literature (Delnoij et al., 1997; Lin et al., 1996; Rensen and Voig, 2001), it can be seen that plume oscillation frequency depends on superficial gas velocity, column width (or diameter), and bubble size (and thus bubble slip velocity). As shown in the present work, plume oscillation frequency was found to be independent of liquid height (or *H/W* ratio). Moreover, as discussed above, our experiments carried out with different spargers indicated that the plume oscillation frequency does not depend on sparger width. Equations 6 and 7 $[f^* \propto (d_B^3/U_B^2)^{-0.5}]$ and correlations of bubble rise velocity and bubble diameter (Clift et al., 1978) indicate that the effect of bubble size on plume oscillation frequency is more pronounced in the smaller bubble diameter range $(d_B < 2.0 \text{ mm})$ than for larger bubbles $(d_B > 2.0 \text{ mm})$. This supports the observations of Buwa and Ranade (2002) that the plume oscillation period for
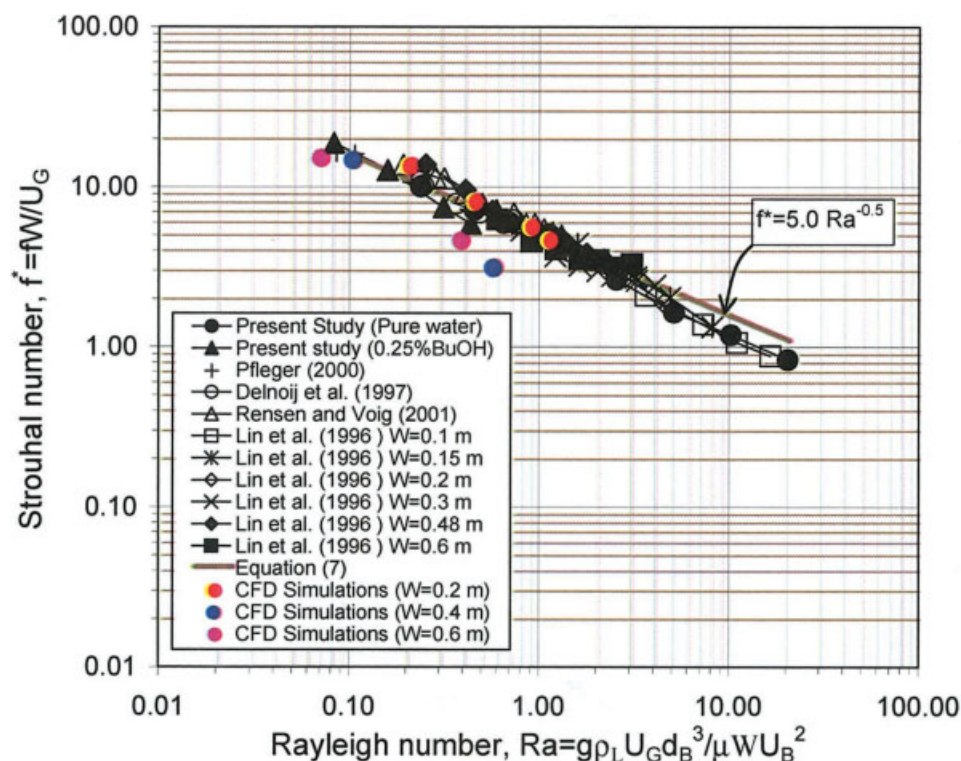
Figure 6. Comparison of present experimental data with experimental data in the literature using dimensionless numbers proposed in the present work and with CFD simulations.

water with 0.25% butanol ($d_B \sim 0.5$–2.0 mm) decreased significantly compared to the plume oscillation period for water ($d_B \sim 4$–8 mm).

Buwa and Ranade (2002) simulated unsteady gas–liquid flows in a rectangular column with the same geometry as that used in the present work. Following their methodology, we carried out additional simulations to evaluate the influence of column width ($W = 0.4$ and 0.6 m, with $H/W = 2.25$, $d_B = 5.0$ mm) and bubble diameter ($d_B = 0.5$ and 20 mm, with $H/W = 2.25$, $W = 0.2$ m) on predicted dynamics. The plume oscillation frequency, obtained from numerically predicted voidage fluctuation time series at different superficial gas velocities, was used to calculate the numerically predicted Strouhal number and is plotted against the Rayleigh number in Figure 6. It was observed that the predictions of Strouhal numbers based on Eulerian–Eulerian simulations showed reasonably good agreement with the values estimated by Eq. 7 for different values of gas velocity and column width. Such validation of CFD models over a wide range of relevant parameters is essential to develop widely applicable CFD models. CFD models validated in such a manner may then be used to simulate practical gas–liquid flows in industrial systems. These experimental and computational studies indicate that more research is needed to understand the role of bubble size and bubble size distribution on dynamics of gas–liquid flows in bubble columns. More detailed experiments with quantitative data on bubble size distribution and its effect of plume oscillation period are needed.

Local voidage fluctuations and bubble passage frequencies

To extract information on low-frequency oscillations, the local voidage signal obtained using the conductivity probe needs to be converted into an instantaneous voidage fluctuation time series. We have calculated local instantaneous voidage over different time scales (τ) and the square of the difference between instantaneous and time-averaged gas holdup (σ) was plotted against the time scale used for averaging. For time scales up to 0.01 s, σ remains constant and corresponds to a gas holdup obtained by passage of single or multiple bubbles. With further increases in the time scale (scale > 0.05 s), the slope of σ vs. τ curve remains constant. With a sufficiently large time scale (>100 s), σ becomes very small and approaches zero.

The instantaneous voidage fluctuation time series generated (from the signal acquired using a standard sparger with H/W ratio of 2.25) using time scales of 0.1 and 1.0 s at superficial gas velocity of 0.16 cm/s is shown in Figure 7a. The low-frequency voidage fluctuations can be clearly seen from the time series. The characteristics time scale 1.0 s was found to capture the low-frequency oscillations satisfactorily. As shown in Figure 7a, the number of low-frequency oscillations was independent of time scales up to 1.0 s. Thus, in all subsequent processing, instantaneous voidage was calculated based on a moving window of 1.0 s. The plume oscillation period was calculated as the reciprocal of characteristic low frequency observed in power spectra of the voidage fluctuation time series. The plume oscillation period for different superficial gas velocities is shown in Figure 7b. The plume oscillation periods
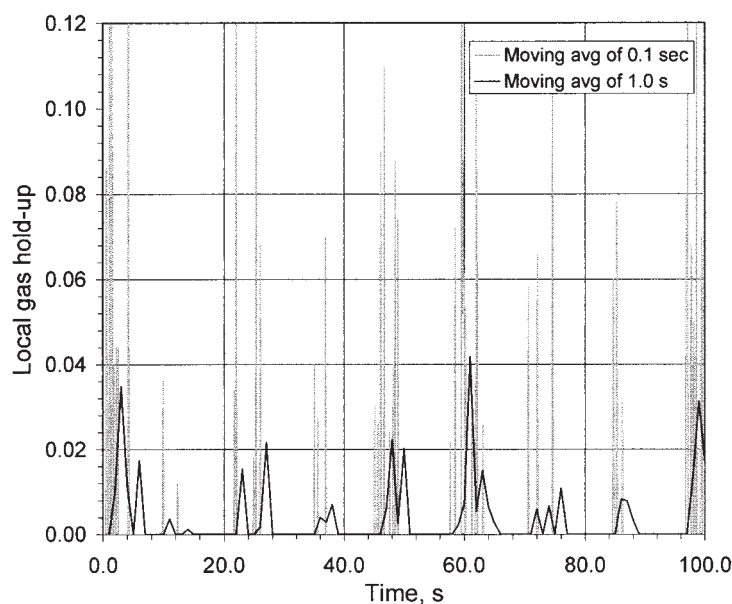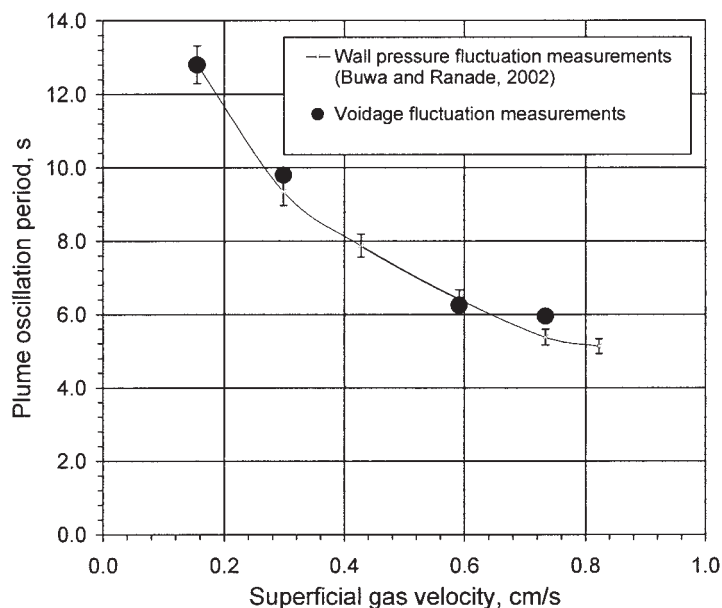
Figure 7. (a) Experimental voidage fluctuation time series recorded at *X* = 0.1 m, *Y* = 0.325 m, and *Z* = 0.025 m obtained at *U$_G$* = 0.16 cm/s; (b) effect of superficial gas velocity on plume oscillation period (standard sparger and *H/W* ratio of 2.25).

obtained using voidage fluctuation time series were in good agreement with those obtained by wall pressure fluctuation measurements. Besides low-frequency oscillations, the experimental voidage fluctuation time series can also be used to extract bubble-scale information such as bubble passage frequency and its distribution as discussed below.

The local time-averaged bubble passage frequencies and their distribution can be calculated using conductivity probes. Typical distributions of bubble passage frequencies at superficial gas velocities of 0.16, 0.73, 6.67, and 11.67 cm/s are shown in Figure 8a–d, respectively (measured at *X* = 0.06 m,

Y = 0.315 m, and *Z* = 0.025 m). It can be seen from the figures that the dominant bubble passage frequencies increase with increasing superficial gas velocity. At lower superficial gas velocities (see Figure 8a and b), a smaller number of bubble clusters was observed (as indicated by the small number of bubbles passing with higher bubble passage frequency). However, with increasing gas flow rate (see Figure 8c and d), a greater number of bubble clusters was observed. The long-time averaged spatial distribution of bubble passage frequency can also be obtained from the distributions shown in Figure 8 (not shown here).
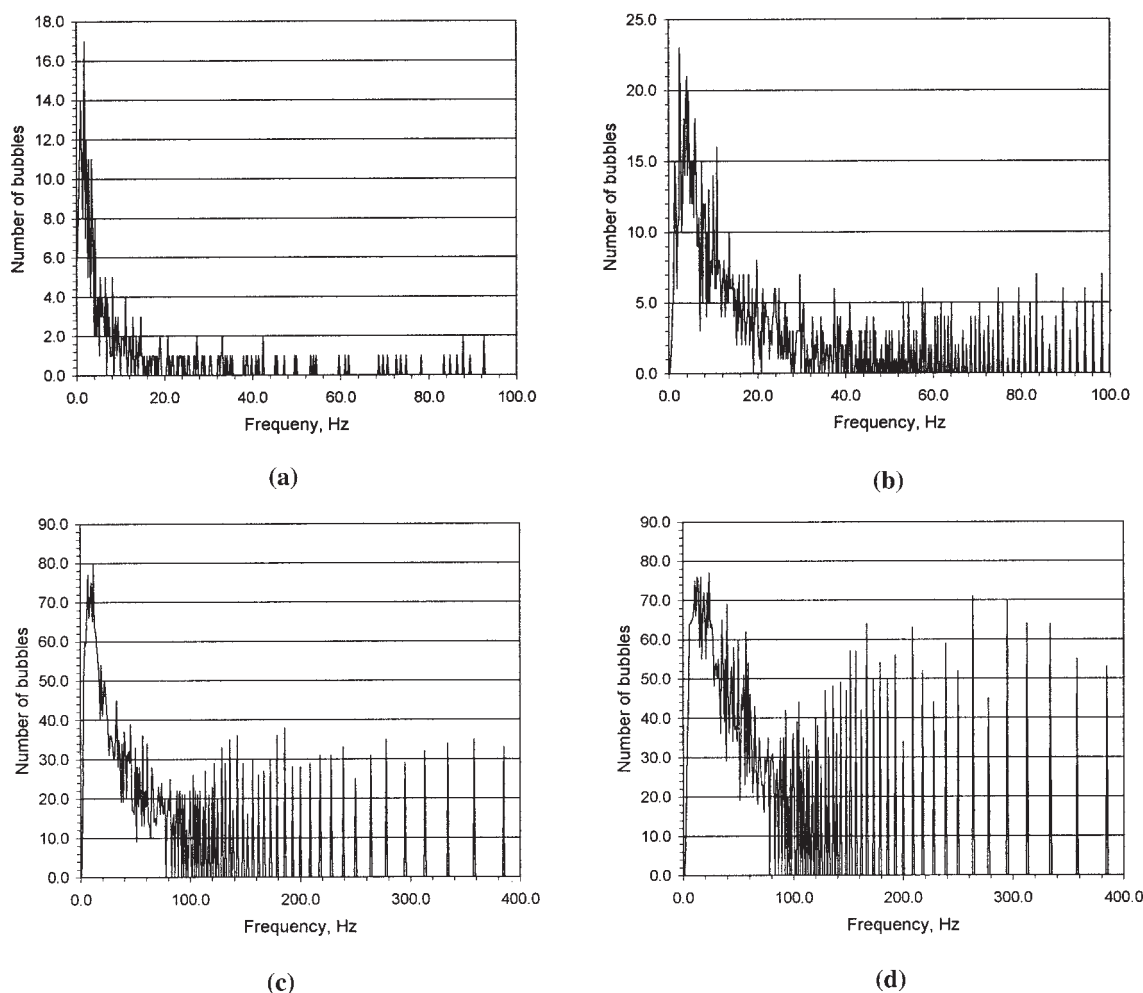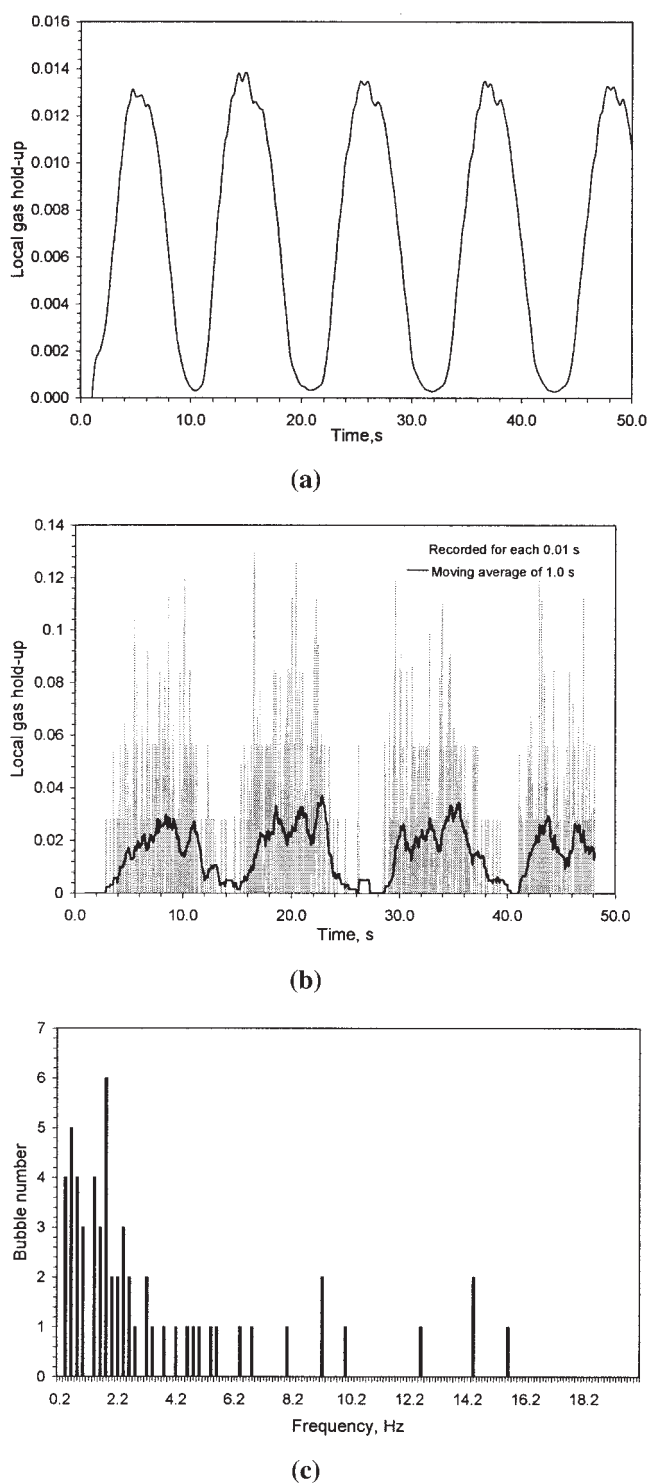
Figure 8. Distribution of bubble passage frequency at (a) 0.16 cm/s, (b) 0.73 cm/s, (c) 6.67 cm/s, and (d) 11.67 cm/s.

$X = 0.06$ m, $Y = 0.315$ m, $Z = 0.025$ m.

Buwa et al. (2002) simulated the motion of bubbles in a rectangular bubble column by solving the force balance over each bubble. The simulated voidage fluctuation time series is shown in Figure 9b. The Strouhal number, calculated from the plume oscillation frequency obtained using Eulerian–Lagrangian simulation, agrees well with Eq. 7 and also with the predictions of Eulerian–Eulerian simulations (predicted voidage fluctuations are shown in Figure 9a). The distribution of bubble passage frequencies obtained using Eulerian–Lagrangian simulation at superficial gas velocity of 0.73 cm/s and recorded at $X = 0.1$ m, $Y = 0.325$ m, and $Z = 0.025$ m is shown in Figure 9c. The experimental bubble passage frequency and its distribution shown in Figure 8 may be used for detailed validation of such detailed bubble-scale information obtained from Eulerian–Lagrangian simulations.

Summary and Conclusions

The dynamics of gas–liquid flows in a rectangular bubble column was characterized using wall pressure and voidage fluctuation measurements. The low-frequency oscillations corresponding to local recirculatory flow were characterized using plume oscillation period. Quantitative information is provided on the influence of superficial gas velocity, H/W ratio, and sparger configuration. The local voidage fluctuations were also used to calculate distribution of bubble passage frequencies. The low-frequency oscillations obtained using voidage fluctuation measurements were in good agreement with wall pressure measurements of Buwa and Ranade (2002). The plume oscillation period was found to decrease with increasing superficial gas velocity and was found to be independent of H/W ratio. It was observed that bubble size distribution produced by the sparger and liquid additives affects the plume oscillation period. Based on the analogy between buoyancy-driven thermal and bubbly flows, a dimensional analysis was carried out to elucidate the quantitative relationship between the characteristic oscillation frequency and various design/operating parameters. This relationship could unify all the data in the literature as well as the present data. Results presented in this work provide the basis for understanding the influence of key system parameters on dynamics of rectangular bubble columns. The results also provide data for validating CFD (Eulerian–Eulerian as well as Eulerian–Lagrangian) models of dispersed gas–liquid flows.

(a)

Recorded for each 0.01 s
—— Moving average of 1.0 s

(b)

(c)

Figure 9. Predicted voidage fluctuation time series.

(a) Eulerian–Eulerian approach; (b) Eulerian–Lagrangian approach; and (c) distribution of bubble passage frequency, obtained using Eulerian–Lagrangian simulation (U_g = 0. 14 cm/s, H/W = 2.25, d_B = 5 mm).

Acknowledgments

Notation

D = column diameter (for cylindrical column), or column depth (for rectangular column), m
d_B = bubble diameter, m
d_h = sparger hole diameter, m
f = plume oscillation frequency, Hz
f^* = Strouhal number
F_b, F_v = buoyancy and viscous force per unit volume, kg m^{-2} s^{-2}
$f_{low,freq}$ = characteristic frequency of low frequency oscillations
g = gravitational acceleration, m/s^2
H = height of liquid, m
l = characteristic length scale, m
L_i = sparger width, m
$M(x,t)$ = phase marker function
$P(f)$ = power contained iin frequency range of f and $f + df$
Ra = Rayleigh number
U_B = bubble rise velocity, m/s
U_G = superficial gas velocity, m/s
W = column width, m
T = time, s

Greek letters

Γ = bubble dispersion coefficient, m^2/s
τ_H = characteristic time scale corresponding to lateral dispersion of bubbles, s
τ_v = characteristic time scale corresponding to the recirculatory motion of a typical circulation cell, s
ρ = density, kg/m^3
μ = viscosity, kg m^{-1} s^{-1}
ε_G = gas holdup

Literature Cited

Becker, S., H. De Bie, and J. Sweeney, "Dynamic Flow Behavior in Bubble Columns," *Chem. Eng. Sci.*, **54**, 4929 (1999).

Becker, S., A. Sokolichin, and G. Eigenberger, "Gas–Liquid Flow in Bubble Columns and Loop Reactors: Part II. Comparison of Detailed Experiments and Flow Simulations," *Chem. Eng. Sci.*, **49**, 5747 (1994).

Briens, L. A., and C. L. Briens, "Cycle Detection and Characterization in Chemical Engineering," *AIChE J.*, **48**, 970 (2002).

Buwa, V. V., V. V. Borkar, and V. V. Ranade, "Development of Conductivity Probes for Characterization of Multiphase Flows," *Proc. of CHEMCON-2001,* Chennai, India (2001).

Buwa, V. V., D. S. Deo, and V. V. Ranade, "Modelling of Gas–Liquid Flows in Bubble Columns: Experiments vs. Eulerian–Lagrangian vs. Eulerian–Eulerian Simulations," *Proc. of 17th Int. Symp. on Chemical Reaction Engineering (ISCRE 17),* Hong Kong, China (2002).

Buwa, V. V., and V. V. Ranade, "Dynamics of Gas–Liquid Flow in Rectangular Bubble Columns: Experiments and Single/Multi-Group Simulations," *Chem. Eng. Sci.*, **57**, 4715 (2002).

Buwa, V. V., and V. V. Ranade, "Mixing in Bubble Column Reactors: Role of Unsteady Flow Structures," *Can. J. Chem. Eng.*, **81**, 402 (2003).

Buwa, V. V., "Modeling of Gas-Liquid Flows in Bubble Columns," PhD Thesis, Indian Institute of Technology-Bombay, Mumbai, India (2004).

Chen, J. J. J., M. Jamialahmadi, and S. M. Li, "Effect of Liquid Depth on Circulation in Bubble Columns: A Visual Study," *Chem. Eng. Res. Des.,* **67**, 203 (1989).

Chen, R. C., J. Reese, and L.-S. Fan, "Flow Structure in a Three-Dimensional Bubble Column and Three Phase Fluidized Bed," *AIChE J.*, **40**, 1093 (1994).

Clift, R., J. R. Grace, and M. E. Weber, *Bubbles, Drops, and Particles*, Academic Press, New York (1978).

Delnoij, E., J. A. M. Kuipers, and W. P. M. van Swaaij, "Dynamic Simulation of Gas–Liquid Two-Phase Flow: Effect of Column Aspect Ratio on the Flow Structure," *Chem. Eng. Sci.*, **52**, 3759 (1997).

Drahos, J., J. Zahradnik, M. Puncochar, M. Fialova, and F. Bradka, "Effect

of Operating Conditions on the Characteristics of Pressure Fluctuations in a Bubble Column," *Chem. Eng. Process*, **29**, 107 (1991).

Kimura, R., and K. Iga, "Bubble Convection," *Mixing in Geophysical Flows*, J. M. Redondo and O. Metais, eds., CIMNE, Barcelona, Spain, pp. 35–51 (1995).

Kumar, S. B., D. Moslemian, and M. P. Dudukovic, "Gas Hold-Up Measurements in Bubble Columns Using Computed Tomography," *AIChE J.*, **43**, 1414 (1997).

Letzel, H. M., J. C. Schouten, R. Krishna, and C. M. van den Bleek, "Characterization of Regimes and Regime Transitions in Bubble Columns by Chaos Analysis of Pressure Signals," *Chem. Eng. Sci.*, **52**, 4447 (1997).

Lin, T.-J., J. Reese, T. Hong, and L.-S. Fan, "Quantitative Analysis and Computation of Two-Dimensional Bubble Columns," *AIChE J.*, **42**, 301 (1996).

Pfleger, D., LDA data, Private communication (2000).

Pfleger, D., and S. Becker, "Modelling and Simulation of the Dynamic Flow Behavior in a Bubble Column," *Chem. Eng. Sci.*, **56**, 1737 (2001).

Pfleger, D., S. Gomes, N. Gilbert, and H.-G. Wagner, "Hydrodynamic Simulations of Laboratory Scale Bubble Columns: Fundamental Studies of the Eulerian–Eulerian Modeling Approach," *Chem. Eng. Sci.*, **54**, 5091 (1999).

Rampure, M. R., V. V. Buwa, and V. V. Ranade, "Modeling of Gas–Liquid and Gas–Liquid–Solid Flows in Bubble Columns: Experiments and CFD Simulations," *Can. J. Chem. Eng.*, **81**, 684 (2003).

Ranade, V. V., and R. P. Utikar, "Dynamics of Gas–Liquid Flow in Bubble Column Reactors," *Chem. Eng. Sci.*, **54**, 5237 (1999).

Rensen, J., and V. Voig, "Experimental Study of the Unsteady Structure of a Confined Bubble Plume," *Int. J. Multiphase Flow*, **27**, 1431 (2001).

Ruzicka, M., J. Drahos, J. Zahradnik, and N. H. Thomas, "Structure of Gas Pressure Signal at Two-Orifice Bubbling from a Common Plenum," *Chem. Eng. Sci.*, **55**, 421 (2000).

Ruzicka, M. C., and N. H. Thomas, "Buoyancy Driven Instability of Bubbly Layers: Analogy with Thermal Convection," *Int. J. of Multiphase Flow*, **29**, 249 (2003).

Sato, Y., and K. Sekoguchi, "Liquid Velocity Distribution in Two-Phase Bubble Flow," *Int. J. Multiphase Flow*, **2**, 79 (1975).

Sunthankar, A. A., and V. V. Ranade, "Dynamics of Gas–Liquid Flow," NCL Internal Project Report (1997).

Tzeng, J.-W., R. C. Chen, and L.-S. Fan, "Visualization of Flow Characteristics in a 2-D Bubble Column and Three-Phase Fluidized Bed," *AIChE J.*, **39**, 733 (1993).

Utikar, R. P., A. A. Sunthankar, and V. V. Ranade, "Characterizing Unsteady Fluid Dynamics of Bubble Column Using Non-Linear Analysis of Wall Pressure Fluctuations," *Ind. Chem. Eng.*, **43**, 16 (2001).

Vial, C., E. Camarasa, S. Poncin, G. Wild, N. Midoux, and J. Bouillard, "Study of Hydrodynamic Behavior in Bubble Columns and External Loop Airlift Reactors Through Analysis of Pressure Fluctuations," *Chem. Eng. Sci.*, **55**, 2957 (2000).

Yao, B. P., C. Zheng, H. E. Gasche, and H. Hofmann, "Bubble Behavior and Flow Structure of Bubble Columns," *Chem. Eng. Process*, **29**, 65 (1991).